JOURNAL OF GEOPHYSICAL RESEARCH, VOL. 114, A08211, doi:10.1029/2008JA013997, 2009

On the character and distribution of lower-frequency radio emissions at Saturn and their relationship to substorm-like events

C. M. Jackman,[1] L. Lamy,[2] M. P. Freeman,[3] P. Zarka,[2] B. Cecconi,[2] W. S. Kurth,[4] S. W. H. Cowley,[5] and M. K. Dougherty[1]

Received 19 December 2008; revised 6 April 2009; accepted 11 May 2009; published 18 August 2009.

[1] With the arrival of the Cassini spacecraft at Saturn in July 2004, there have been quasi-continuous observations of Saturn kilometric radiation (SKR) emissions. Exploration of the nightside magnetosphere has revealed evidence of plasmoid-like magnetic structures and other phenomena indicative of the Kronian equivalent of terrestrial substorms. In general, there is a good correlation between the timing of reconnection events and enhancements in the auroral SKR emission. Eight of nine reconnection events studied occur at SKR phases where the SKR power would be expected to be rising with time. Thus, while the recurrence rate of substorm-like events at Saturn is likely much longer than the planetary rotation timescale, the events are favored to occur at a particular phase of the rotation. We show three examples in each of which the SKR spectrum extends to lower frequencies than usual. This can be interpreted as an expansion of the auroral particle acceleration region to higher altitudes along magnetic field lines as a direct consequence of an increase in the magnetosphere-ionosphere current density driven by substorm-like events. We then conduct a survey of such low-frequency extensions during the equatorial orbits of 2005–2006 and place some constraints on visibility of these radio emissions.

Citation: Jackman, C. M., L. Lamy, M. P. Freeman, P. Zarka, B. Cecconi, W. S. Kurth, S. W. H. Cowley, and M. K. Dougherty (2009), On the character and distribution of lower-frequency radio emissions at Saturn and their relationship to substorm-like events, *J. Geophys. Res.*, *114*, A08211, doi:10.1029/2008JA013997.

1. Introduction

[2] The substorm phenomenon has been widely studied at the Earth for many years. It is a way for magnetic energy to be released in the nightside magnetosphere with a wide variety of consequent changes observed in the aurora, magnetic field, energetic particles, electrical currents, and convection [e.g., *Akasofu*, 1964; *Russell and McPherron*, 1973; *Angelopoulos et al.*, 2008]. Reconnection events associated with substorms are generally identified by sharp changes in the north/south component of the magnetic field, corresponding to dipolarizations of the field, or plasmoids passing the spacecraft. These signatures are often accompanied by strong plasma flows and plasma energization [e.g., *Nakamura et al.*, 2002]. In addition, remote diagnostics such as global energetic neutral atom fluxes have also been investigated [e.g., *Brandt et al.*, 2002; *Mitchell et al.*, 2003; *Fok et al.*, 2006]. More recently, the dynamics of the magnetotails of Jupiter and Saturn have become a topic of great interest with some similar substorm-like signatures being observed in situ [e.g., *Kronberg et al.*, 2005, 2007; *Jackman et al.*, 2007, 2008]. Here we will focus on the relationship between substorm-like events observed in situ in Saturn's magnetotail and remote sensing of Saturn's radio emissions. We will explore enhancements in the intensity of radio emissions coincident with substorm-like events and also explain the link between lower-frequency emissions and the motion of radio sources.

1.1. Terrestrial Radio Emissions and Substorms

[3] A direct relationship has been observed between the intense radio emission from the Earth's auroral regions called auroral kilometric radiation (AKR) and substorms [*Benediktov et al.*, 1968; *Gurnett*, 1974; *Kurth et al.*, 1975; *Kaiser and Alexander*, 1977]. Substorms cause abrupt acceleration of particles along magnetic field lines which map into the auroral zones and help drive the westward substorm (DP1) electrojet. These particles can also generate AKR by the cyclotron maser instability (CMI) [e.g., *Wu and Lee*, 1979] on field lines at geocentric distances of $\sim$2–4 R_E. While the average power of AKR is found to increase with substorm activity, the correlation is not always perfect, primarily due to visibility effects. In general, AKR provides a good indication of magnetic substorm activity, provided the measurements are taken within the regions of primary illumination for the AKR, and at distances

[1]Blackett Laboratory, Imperial College London, London, UK.
[2]LESIA, Observatoire de Paris, Université Paris Diderot, UPMC, CNRS, Meudon, France.
[3]British Antarctic Survey, Cambridge, UK.
[4]Department of Physics and Astronomy, University of Iowa, Iowa City, Iowa, USA.
[5]Department of Physics and Astronomy, University of Leicester, Leicester, UK.

0148-0227/09/2008JA013997$09.00

sufficiently remote from the Earth to avoid local propagation cutoff effects associated with the shadow zone [*Voots et al.*, 1977; *Green et al.*, 1977]. Recent work has focused on deciphering the precise beaming characteristics of the AKR and implies that AKR observations from remote locations sample only a small part of the auroral oval from any given location [*Mutel et al.*, 2008].

[4] The frequency of the AKR emission, f, is related to the position of the radio source along the field line, due to the fact that the emission is generated at or close to the local electron cyclotron frequency, f_{CE}, which in turn is proportional to the total field strength. Substituting the formula for dipole magnetic field strength into the equation for the electron cyclotron frequency and rearranging, we find

$$\frac{R}{R_P} = \left(\frac{eB_{eq}\sqrt{1+3\mathrm{Sin}^2\lambda}}{2\pi m_e f} \right)^{\frac{1}{3}} \quad (1)$$

where R_P (=6371 km) is the planetary radius, R is the distance from the planet's center, λ is the magnetic latitude, B_{eq} = 31,100 nT is magnetic field strength at the planet's surface on the equator, e is the electron charge, and m_e is the electron mass. Figure 1, reproduced from *Lamy et al.* [2008] (hereinafter referred to as L08), is a schematic diagram of radio emissions from Saturn but is also applicable to Earth and Jupiter. It illustrates the beaming characteristics and shadow zones mentioned above, along with the relationship between emission frequency and source altitude on a field line.

[5] The AKR shows abrupt frequency expansion into lower (and sometimes higher) frequencies at substorm onset [*Kaiser and Alexander*, 1977; *Anderson et al.*, 1997, 1998]. Using Polar plasma wave instrumentation (PWI) observations, *Morioka et al.* [2007] identified two source regions at substorm onset. The higher-frequency ($\sim$300–500 kHz) component of AKR ("MF-AKR") seems to persist before, during, and after substorm onset and is seemingly largely insensitive to the moment of substorm onset. The lower-frequency ($\sim$30–150 kHz) component of AKR ("LF-AKR") abruptly appears at substorm onset, with a sudden frequency expansion, explosive amplitude growth, and little frequency drift. *Morioka et al.* [2008] suggested that these AKR breakup signatures indicate the abrupt formation at the substorm onset of a new high-altitude field-aligned particle acceleration region between $\sim$8000 and 18,000 km altitude, consistent with equation (1) for emissions within the auroral oval at $\lambda \sim 70°$ latitude.

[6] We suggest that the physical mechanism behind extension of the radio emission to lower frequency following substorms may be explained as follows: Substorms generate field-aligned currents in the auroral zones whose density may exceed the maximum value that can be carried by magnetospheric electrons without acceleration. This is given by

$$j_{\|i0} = eN\left(\frac{W_{th}}{2\pi m_e}\right)^{1/2}, \quad (2)$$

where the magnetospheric electron population has been assumed to be an isotropic Maxwellian of density N and thermal energy W_{th}. This expression corresponds to the case of a full downward going loss cone and an empty upward going loss cone. Under such conditions of strong upward field-aligned current enhancement, and according to *Knight*'s [1973] kinetic theory, a field-aligned voltage must exist along the auroral field lines which accelerates magnetospheric electrons into the ionosphere to produce the required current. We might plausibly expect that the auroral and radio sources will be stimulated by this precipitation. The extent of the field-aligned voltage drop is directly related to the field-aligned current density [e.g., *Cowley et al.*, 2004], and the minimum distance of the "top" of the voltage drop is given by

$$\left(\frac{r_{\min}}{R_i}\right) \approx \left(\frac{j_{\|i}}{j_{\|i0}}\right)^{1/3} \quad (3)$$

where R_i is the radial distance of the ionospheric current layer. Thus we suggest that the extension of the auroral acceleration region to higher altitude is a direct consequence of the strong field-aligned currents and associated electron precipitation which can be driven by substorms. AKR is generated at or close to the local electron cyclotron frequency, which in turn is proportional to the total field strength. Thus for an acceleration region at higher altitude, the radio emissions have characteristically lower frequency.

[7] The existence of a low-altitude (MF-AKR) acceleration region between $\sim$3000 and 5000 km altitude seems to be a necessary condition for the ignition of the high-altitude bursty acceleration discussed by *Morioka et al.* [2007]. Sixty four of 92 events (69.5%) studied by *Morioka et al.* [2007] were either dual source or wide source, indicating that the appearance of a new AKR source region on a higher-altitude auroral field line is a common feature at terrestrial substorm onset. This raises the question: do similar processes occur at other planets?

1.2. Jovian Radio Emissions and Energetic Events

[8] Magnetic field and energetic particle data suggest that Jupiter's magnetosphere is periodically affected by large-scale energetic phenomena which are analogous to terrestrial substorms [e.g., *Krupp et al.*, 1998; *Woch et al.*, 1998; *Kronberg et al.*, 2005, 2007]. *Louarn et al.* [1998] presented evidence for a link between such substorm-like events (as evidenced particularly by plasma sheet thinnings) and low-frequency Jovian radio emissions. Subsequently, *Louarn et al.* [2000] surveyed $\sim$9 months of Galileo data and found that the substorm-like events correspond to global increases in the flux of various radio emissions and to spectral/temporal modifications in their morphology. They characterized these radio emissions using two identification criteria: the simultaneous observation of an increase in the flux of the auroral radio emissions and the creation of a new source of n-KOM (a low-frequency component of the Jovian radio emission). They identified 32 events during 130 days of observation distributed over a 245-day period and found this corresponds to an average recurrence time of 3.8 days.

[9] In this paper we will now focus our attention on the Kronian system and observe how Saturn kilometric

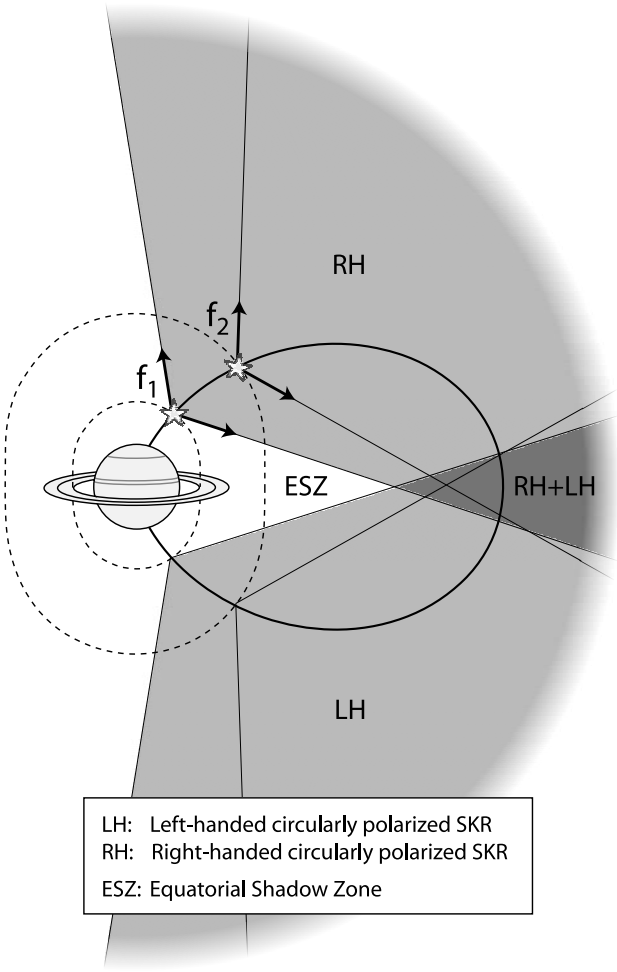

Figure 1. Schematic illustrating the equatorial shadow zone produced by anisotropic beaming of SKR. Stars represent radio sources at two frequencies ($f_1 \geq f_2$) along the same magnetic field line (solid line). Radio emission is beamed along a hollow cone (black arrows). The dashed lines represent the isocontours corresponding to $f = f_{ce}$. Figure reproduced from *Lamy et al.* [2008, Figure 7].

radiation (SKR) emissions compare with AKR and Jovian emissions in their response to substorm-like events.

1.3. Kronian Radio Emissions and Magnetospheric Dynamics

[10] Prior to the arrival at Saturn of the Cassini spacecraft on 1 July 2004, remote sensing studies of the planet's radio emissions, specifically of SKR, were the primary source of information concerning the dynamics of Saturn's magnetosphere and its interaction with the solar wind. SKR was detected by the Planetary Radio Astronomy (PRA) experiment on Voyager-1 in 1980 [*Kaiser et al.*, 1980]. It is analogous to terrestrial AKR, with a spectrum that spreads from ~3 kHz to 1.2 MHz, with the broad peak generally located between 100 and 400 kHz [e.g., *Kaiser et al.*, 1984]. Similar to AKR, SKR is believed to be generated by the CMI in the auroral acceleration region and indeed appears to be associated with UV aurorae caused by the precipitation into the atmosphere of accelerated electrons with energies in the range ~1–20 keV [*Cowley et al.*, 2004]. *Cecconi et al.* [2009] show that southern SKR sources are distributed along magnetic field lines with footprints between −80 and −65°, encompassing the main auroral oval which typically lies between −70 and −75° latitude in quiet magnetospheric conditions [*Badman et al.*, 2006].

[11] Strong correlations have been found between SKR emission and solar wind dynamic pressure modulations [e.g., *Desch and Rucker*, 1983; *Taubenschuss et al.*, 2006]. In January 2004, a joint Hubble Space Telescope (HST) and Cassini campaign was undertaken which included concurrent measurements of the solar wind and interplanetary magnetic field (IMF), SKR emissions, and Saturn's UV aurora. Following a solar wind compression, the auroral oval was observed to brighten and expand significantly poleward [e.g., *Clarke et al.*, 2005] and the usual modulation of SKR at about the planetary rotation period was disrupted. Specifically, the SKR emissions were found initially to intensify with a spectrum that spread to lower frequencies followed by a period of quiet SKR [*Jackman et al.*, 2005]. However, *Kurth et al.* [2005] noted that the Unified Radio and Plasma Wave experiment on board the Ulysses spacecraft detected SKR during this period. This suggests that the effect of the solar wind compression was initially to intensify the SKR emissions and then subsequently disrupt their beaming pattern, such that they could not be observed by Cassini. This is supported by *Badman et al.* [2008] who studied the pattern of SKR during 2003–2004, while Cassini was still upstream of Saturn, and following Saturn orbit insertion (SOI) during Cassini Rev A in the solar wind. They found that magnetospheric compressions generally produced intense bursts of SKR but did not otherwise significantly alter the pulsing of the emission.

[12] *Cowley et al.* [2005] suggested that such auroral and SKR effects can be due to bursts of rapid magnetotail reconnection induced by shock compressions of the magnetosphere. This was investigated by *Bunce et al.* [2005] who explored the behavior of the SKR during the SOI pass in July 2004 and identified a strong burst of SKR coincident with a magnetic field disturbance and hot plasma acceleration symptomatic of tail reconnection. The burst of SKR extended down to lower frequencies and disturbed the previous planetary-modulated radio emissions, which then reasserted themselves after several cycles. Thus the SOI behavior was similar to that observed in January 2004, with the added benefit of in situ fields and particles measurements from which the reconnection mechanism could be inferred.

[13] Since 2004, Cassini has completed many orbits of the Kronian magnetosphere, and these have afforded us a chance to study magnetotail dynamics in much more detail than before. Using data from the Cassini magnetometer, *Jackman et al.* [2007] found three more examples of tail reconnection events in situ, while *Jackman et al.* [2008] then supplemented this work with a multi-instrument study of these three events plus an additional two. In general, tail reconnection events and the resultant passage of plasmoids are associated with strong magnetic perturbations and bursts of energetic particles and thus have strong parallels with reconnection within terrestrial substorms in terms of their observable effects.

[14] Rapid reconnection can also result in the production of energetic neutral atoms (ENAs) via charge exchange with the energetic particles produced. *Mitchell et al.* [2005] found that strong ENA fluxes indicative of an Earth-like substorm process typically emanate from the region of $\sim$20–30 R_S. They suggested this radial range as the likely typical location of the reconnection site and found in turn that strong ENA fluxes from this region were well correlated with enhancements in SKR. *Hill et al.* [2008] studied the pattern of ENA emissions prior to a known reconnection event in the Kronian tail and were able to pinpoint the source of energization and hence the likely reconnection site to $\sim$26 R_S downtail.

[15] Thus the link between solar wind-driven aurorae, reconnection, substorms, and SKR emissions appears to be a strong one. In this paper, we will focus on the relationship between in situ observations of substorm-like events on Saturn's nightside, and the resultant SKR emissions. In section 2 we outline the data sets used, while in section 3 we show three case studies of magnetic field and SKR data from the deep tail orbits of 2006. In section 4 we explore in detail the typical character of the low-frequency part of the SKR spectrum, the visibility factors that impact its interpretation, and its possible links to dynamic nightside processes.

2. Data Set

[16] For this paper, we combine data from the Cassini magnetometer (MAG) [*Dougherty et al.*, 2004] with that from the Cassini Radio and Plasma Wave Science (RPWS) instrument [*Gurnett et al.*, 2004]. As mentioned above, the MAG data are used to identify reconnection events in the magnetotail which are typically indicated by northward/southward turnings of the field. These can often be accompanied by signatures of angular momentum conservation, as plasma speeds up/slows down in response to reconnection and resulting reconfiguration of the field on the nightside.

[17] We use the RPWS data to provide information about the SKR, which is an extremely useful diagnostic of global magnetospheric dynamics. The data set we use is an extension of that derived by L08 and based on previous work by *Zarka et al.* [2004] and *Cecconi and Zarka* [2005]. L08 calibrated the near-continuous RPWS data from SOI onward and derived the intensity and circular polarization state of the observed radio waves as a function of time and frequency. The processed data comprise a spectrum every 180 s, consisting of 24 logarithmically spaced channels between 3.5 and 300 kHz (with $\Delta f/f = 20\%$) and 24 linearly spaced channels (with δf = 50 kHz) between 350 and 1500 kHz. The specific products used in this paper are the received flux density (in W m^{-2} Hz^{-1}) normalized to 1 AU and the emitted power (in W sr^{-1}).

2.1. Visibility of Radio Emissions

[18] The key to careful interpretation of radio data is an understanding of the role of visibility effects, which are highly dependent on spacecraft location. As mentioned above, the SKR spectrum typically extends from a few kHz to 1200 kHz, with a peak between 100 and 400 kHz. On the basis of 2.75 years of post-SOI data, L08 found that the R-X mode is the dominant mode of emission, but Cassini also detected some weaker L-O mode emissions. Goniopolarimetric (direction finding) measurements confirm that right-hand (RH) polarized emission comes from the Northern Hemisphere, with left-hand (LH) coming from the south. LH and RH spectra are conjugate with respect to spacecraft latitude (λ_{SC}), and thus they are added together in the data processing to derive the average variations of SKR visibility.

[19] While SKR is observed quasi-continuously, there are strong variations of visibility as a function of observer position, both in local time (LT) and latitude. In general, the variable visibility along Cassini's orbit is consistent with sources at or close to the local electron cyclotron frequency f_{ce} in the LT sector 0900–1200 h and at latitudes $\geq$70°. Measured SKR intensities are generally larger on the dawn-side, with weakest emissions observed between 16 and 20 h. However, we note that SKR can be observed from a large range of LT, not just restricted to the dawn-to-noon sector [e.g., *Cecconi et al.*, 2009]. *Farrell et al.* [2005] observed SKR during the nightside passage of SOI which they claim originated from the near-midnight region of field lines near L$\sim$10–15. This suggests the presence of an active region in the nightside inner magnetosphere.

[20] The main visibility constraint with radial distance arises due to the anisotropic nature of the emission, which is thought to be beamed along hollow cones centered on the local magnetic field vector. L08 found that this beaming results in the existence of an equatorial shadow zone as illustrated schematically in Figure 1 (out to radial distance of $\sim$4 R_S at 169 kHz and $\sim$6–7 R_S at 80 kHz). Additionally, SKR visibility is known to be affected by observer latitude, with maximum SKR intensity and frequency extent being observed between 20 and 40°. At much higher latitudes (>$\sim$55°), L08 reported a systematic disappearance of SKR at high frequencies. Modeling work has simulated this disappearance by assuming the SKR sources are colocated with the UV auroral oval [*Lamy*, 2008].

2.2. Lower-Frequency Components

[21] While the SKR spectrum may be most intense in the range $\sim$100–400 kHz [L08], there are also two well defined lower-frequency components to Saturn's radio spectrum, both of which are preferentially observed from high latitudes and are modulated at or close to the SKR rotational periodicity. The first is n-SMR (narrowband Saturnian Myriametric Radiation), named by *Louarn et al.* [2007]. This is an intense but weakly polarized emission that appears below 10 kHz. The second is a narrowband kilometric component (n-SKR) which extends mainly between 10 and 40 kHz but sometimes as low as 3 kHz. It corresponds to the narrowband electromagnetic emissions first reported by *Gurnett et al.* [1981] and is less intense than the main SKR and the n-SMR, with a peak at $\sim$20 kHz. L08 have suggested that it is indeed a separate feature of Saturn's radio spectrum, based on observation of the polarization of the emissions. Z. Wang et al. (Cassini observations of narrowband radio emissions in Saturn's magnetosphere, submitted to *Journal of Geophysical Research*, 2008) and *Ye et al.* [2009] investigated the source of the narrowband emissions in the frequency range of 5–30 kHz and noted that the narrowband emissions often occur near 5 kHz, with other apparently associated bands between 20 and 30 kHz. While *Louarn et al.* [2007] have shown that these emissions can be intensified following an increase in SKR intensity and

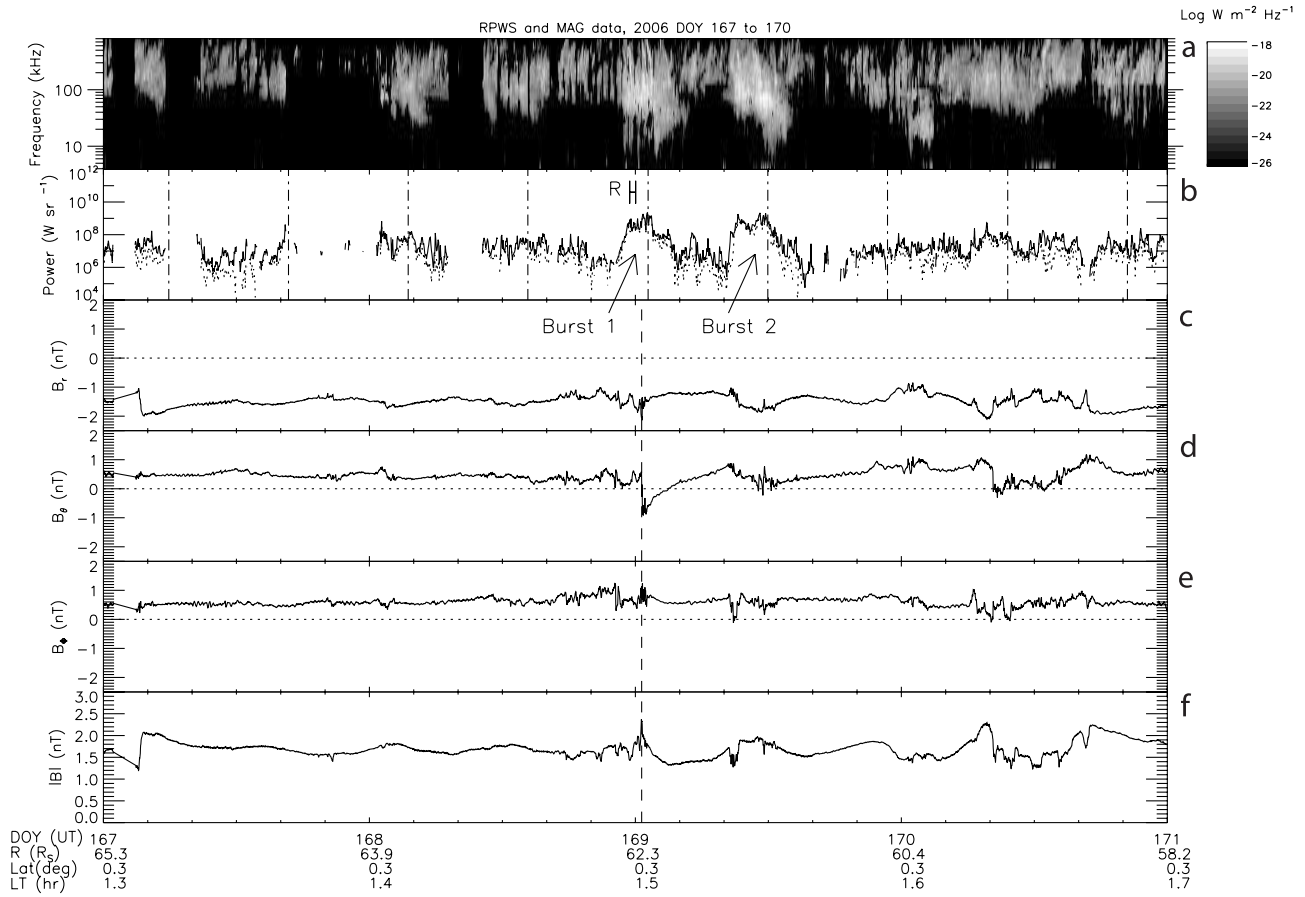

Figure 2. RPWS and MAG data from day 167–170, 2006, showing (a) a frequency-time spectrogram of the radio emissions and (b) the band-integrated SKR power across 4–1000 kHz (solid line) and 100–300 kHz (dashed line) ranges. (c–f) Also shown are the magnetic field components in KRTP coordinates and total magnetic field strength. Trajectory information is given at the bottom.

bandwidth, it is not the purpose of this paper to address these emissions. Rather, we focus on the expansion of the main band of auroral SKR to lower frequencies and its growth to larger intensities, in response to substorm-like events.

3. Case Study Examples

[22] In this section we show three case study examples of known reconnection events in Saturn's magnetotail. The MAG data for two of these events have been discussed by *Jackman et al.* [2008] but here we show the corresponding RPWS data and study the correlation between these substorm-like events and SKR emissions.

3.1. Example A: Day 169, 2006

[23] Figure 2 shows data from day 167–170 2006. Figure 2a shows a frequency-time spectrogram of radio emission from the RPWS instrument, over the frequency range 3.9–800 kHz, with flux values corresponding to the grayscale on the right of the plot. Figure 2b shows the emitted SKR power normalized to 1 AU in Watts per steradian, with the solid line showing the power integrated over the 4–1000 kHz range and the dotted line showing the 100–300 kHz range. Vertical dot-dashed lines indicate the times when Cassini is at 100° subsolar longitude in the *Kurth et al.* [2008] longitude system, around which SKR is expected to maximize on average. Figures 2c–2e show the radial, theta, and azimuthal components of the magnetic field in KRTP coordinates. In this system, the radial component (B_r) is positive outward from Saturn, the theta component (B_θ) is positive southward, and the azimuthal component (B_φ) is positive in the direction of corotation. Figure 2f shows the total magnetic field strength. Universal time, radial distance, latitude, and local time are given beneath the plot.

[24] Cassini observed a traveling compression region (TCR) at 0034 UT on day 169 (18 June), when the spacecraft was at ~62.29 R_S downtail, 1.5 h LT, and a latitude of 0.3° [*Jackman et al.*, 2008], and this time is marked on Figures 2c–2f by a vertical dashed line. TCRs are magnetic signatures observed in the lobe, thought to be caused by localized bulges in the plasma sheet due to the formation and rapid movement of plasmoid-type flux ropes down tail [e.g., *Slavin et al.*, 1984]. Ideally we would like to know the timing and location of the reconnection event that spawned this plasmoid. However, in order to calculate plasmoid speeds, we need reliable ion moments from the CAPS Ion Mass Spectrometer (IMS), and extraction of these is complicated by several factors. In this case, velocity data was not available, so in order to obtain a rough estimate of the timing of the reconnection event, we make some assumptions based on the work of *Hill et al.* [2008]. They

used available ion velocity data combined with ENA fluxes to deduce the reconnection site location and plasmoid speed for one event in 2006. They found the maximum measured ion flow speed for the plasmoid was ~800 km/s, with a reconnection site location near ~30 R_S. They placed an upper limit of ~1000 km/s on the tailward speed of the O-line, and an average of ~500 km/s on the X-line speed. If we assume 800 km/s as a plasmoid speed and work backward from our TCR observation at ~62.29 R_S, we find a travel time of 40 min 32 s for a plasmoid released at 30 R_S to reach Cassini. Thus as a rough estimate based on the available data, we might expect the reconnection event to have occurred on day 168 at ~2354 UT. In Figure 2b, we have bracketed this time with error bars (corresponding to plasmoid speeds of 500–1000 km/s), thus marking out a plausible interval during which the reconnection event, "R," may have occurred.

[25] Returning to Figure 2a, we note that the SKR emissions are relatively quiet for day 167 and most of day 168 and there are several intervals where no emission is observed. The emissions during this period are largely confined to the ~100–400 kHz band, where the bulk of the SKR emission is typically observed, and the average integrated power over this range is of order 1×10^7 W sr^{-1}. However, at the end of day 168 there is a very strong burst of SKR emission, with maximum power of 2.2×10^9 W sr^{-1}, and an extension to frequencies below 10 kHz. This burst lasts for more than 4 h and is followed by a second, slightly smaller burst on day 169, which peaks at 2×10^9 W sr^{-1} and also exhibits extension to low frequencies. This second burst is then followed by a period of quiet SKR with average powers more than 2 orders of magnitude smaller than the previous bursts. The emissions reassert themselves from the start of day 170, with average powers for that day exceeding 1×10^7 W sr^{-1}.

[26] We note that the first large burst (end of day 168) occurred before the observation of the TCR but close to the possible timing of the reconnection event itself. This could occur if energetic electrons produced during the reconnection event precipitated into the auroral zones and triggered SKR nearly instantaneously, before the plasmoid had time to travel to the deep magnetotail to result in the observed magnetic signature. We suggest that the character of the emissions observed here is similar to that reported for AKR by *Morioka et al.* [2007]. As discussed in section 1.1, they observed two bands of AKR emission: one at higher frequencies that is largely insensitive to substorm onset and another at lower frequencies which appears abruptly at substorm onset. It seems plausible to suggest that the data we show here follow a similar pattern, with quasi-continuous higher-frequency emission before, during, and after the observation of the TCR, and a strong extension of the spectrum to lower frequency prior to the observation of the TCR but around the projected onset time of this substorm-like reconnection event.

[27] We note also that *Morioka et al.* [2007] suggested several scenarios for AKR source motion that resulted in the "dual-component" AKR spectra they observed coincident with terrestrial substorms. As SKR is emitted close to the f_{CE}, which is directly proportional to magnetic field and thus to altitude, the frequency we observe can be related directly to source altitude (as detailed in section 1.3 above). We thus expect that sources higher along the field lines are responsible for the low-frequency extensions we observe here. Goniopolarimetric (direction-finding) tools have been developed [*Cecconi et al.*, 2009] to analyze the characteristics of the SKR sources, with overall accuracy on direction of arrival of order 2°. Unfortunately, as Cassini was more than 60 R_S downtail during this observation, it was not possible to use these tools to accurately resolve the source locations of the radio emissions. Nevertheless, on the basis of emission from the center of the main auroral oval (72°, see section 1.3) at the electron cyclotron frequency in a dipole Kronian magnetic field with equatorial field strength 20 μT, we would predict from equation (1) that the quasi-continuous emissions between ~100 and ~400 kHz come from a Kronian-centric distance of 1.4–2.2 R_S and the lower-frequency extension down to ~10 kHz reaches to a distance of 4.8 R_S.

[28] On examination of the SKR emissions over the full interval shown in Figure 2, we note that the peak integrated powers for the two large bursts surrounding the TCR observation were an order of magnitude higher than the peak powers for the surrounding days. However, the large bursts did not appear to disrupt the pattern of planetary phasing as outlined by the vertical dashed lines. Periods of strong SKR emissions have been shown by both Voyager and Cassini to be consistent with the impact of solar wind compressions on the magnetosphere and suggested by several authors to be associated with possible dynamics in the magnetotail [e.g., *Cowley et al.*, 2005; *Bunce et al.*, 2005]. However, the occurrence or otherwise of a solar wind compression cannot be confirmed without the presence of an upstream monitor, and as noted by *Badman et al.* [2008], even large solar wind compressions do not necessarily result in "out of phase" SKR bursts.

3.2. Example B: Day 060, 2006

[29] Figure 3 shows RPWS and MAG data from day 58–61 2006, in the same format as Figure 2. Cassini executed a close flyby of Titan on day 058 at ~0825 UT and the magnetic signature is visible in all components. Following that, the data showed a regular pattern of periodic current sheet encounters (evidenced by a zero radial component at the center of the sheet). For the purposes of this discussion we may assume that Cassini is essentially stationary with respect to the current sheet, which is flapping across the spacecraft with a periodicity linked in some way to the planetary rotation rate [e.g., *Khurana et al.*, 2009; *Jackman et al.*, 2009; C. S. Arridge et al., manuscript in preparation, 2009]. On day 059 at ~0800 UT the current sheet moves across Cassini, and the radial field component on the opposite side of the sheet is ~+2 nT. The next encounter is later that day at ~1900 UT, where, despite the spacecraft maintaining the same latitude, the positive excursion of the radial component is less than 2 nT. The next encounter with the current sheet is on day 060 at ~0500 UT. This time the radial component just reaches zero, indicating that the current sheet has just briefly touched Cassini as it moved down toward the spacecraft. During the interval encompassing these three current sheet encounters, Cassini moved tailward ~5 R_S, keeping a constant spacecraft latitude. These progressively decreasing passes through the center of the sheet may either indicate a decrease in the degree

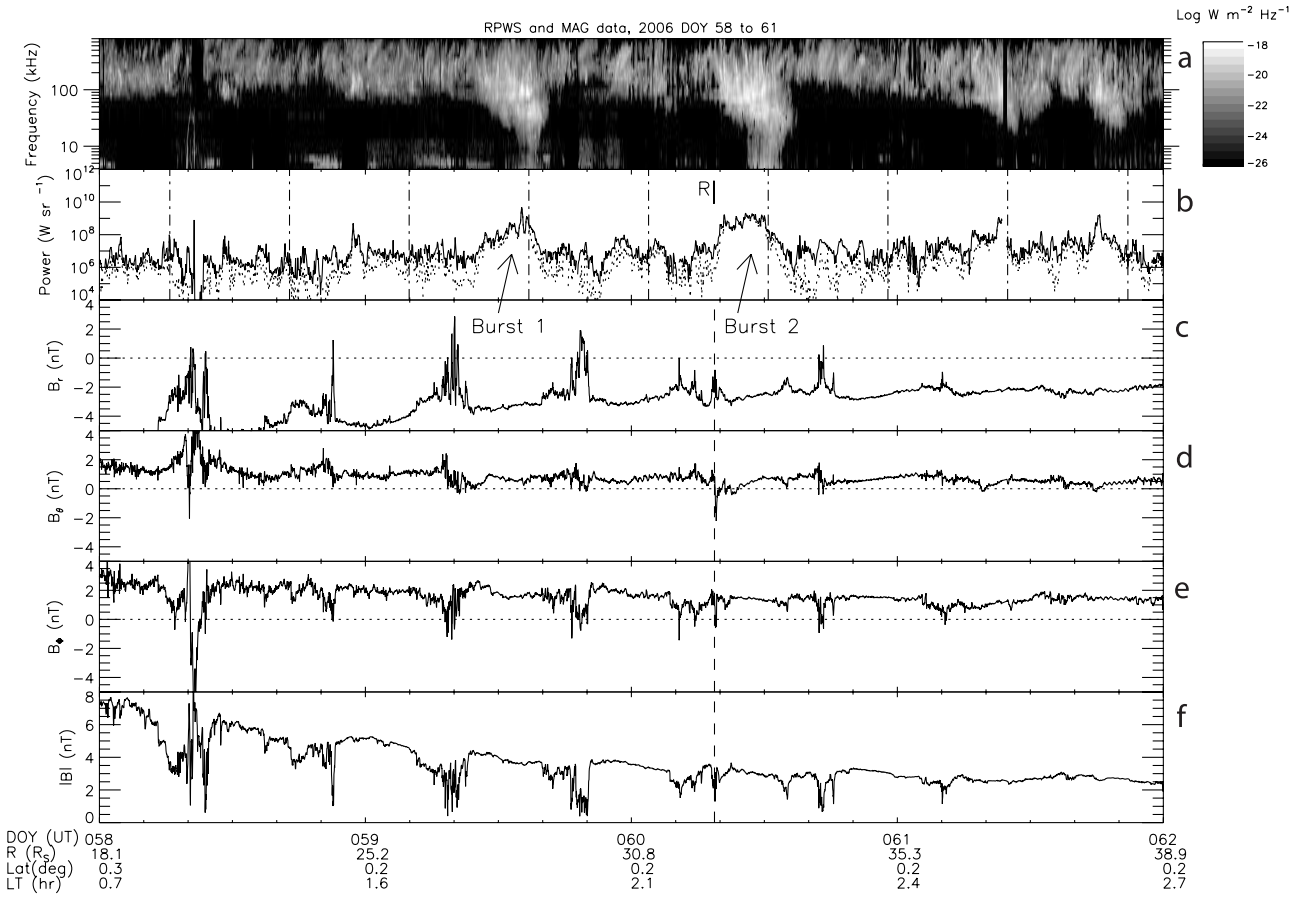

Figure 3. RPWS and MAG data from day 58–61, 2006, in the same format as Figure 2.

of current sheet flapping or a progressively thinning current sheet, both spatially with increasing radial distance, and temporally, suggesting the onset of a reconnection event. Indeed, on day 060 at ~0730 UT, Cassini observed a plasmoid signature in the form of a sharp northward turning of the magnetic field. A vertical dashed line through Figures 3c–3f shows this timing. As this plasmoid was observed at a radial distance of ~32 R_S, we suggest that it was released during a reconnection event planetward of this position.

[30] Looking to Figures 3a and 3b, we note that throughout the entire 4-day period shown here, there is nearly constant SKR emission in the ~100–400 kHz frequency band. On day 059 between ~1200 and 1700 UT there is a continuous extension of the emission to the lowest-frequency channels. The burst occurs exactly in phase with the expected pulsing shown by the vertical dashed lines in Figure 3b, and the SKR power at this time peaks at $\sim 4.8 \times 10^9$ W sr^{-1}. There is then a second, broader burst of SKR with low-frequency extension on day 060 from ~0830 to 1500 UT, peaking at $\sim 1.9 \times 10^9$ W sr^{-1}. The low-frequency extension associated with this burst occurs in phase with the predicted pulsing. Again, these emissions have similar character to those reported with AKR data at the Earth by *Morioka et al.* [2007]. The peak intensities of the fluxes during the SKR bursts of day 059 and day 060 are significantly higher (by about an order of magnitude) than the surrounding peak fluxes.

[31] As for example A, we have calculated the expected timing of the reconnection event associated with the observed plasmoid, using an assumed source at 30 R_S and incorporating the velocity estimates of *Hill et al.* [2008]. For a plasmoid velocity of 800 km/s, we obtain a reconnection event time of ~0727.55 UT, and this is shown in Figure 3b. The error bars to represent upper and lower velocity estimates of 500 and 1000 km/s are omitted as they are too close to the value at ~0727.55 UT to be seen on the scale of this plot. The expected timing of the reconnection event coincides closely with the onset of the strong burst of emission on day 060. We thus suggest that, in a similar way to example A, the process of magnetic reconnection has stimulated SKR emissions which have been observed to extend to the lower reaches of the spectrum, implying the spread in altitude of the radio sources in response to precipitating energized electrons. However, the cause of the first large burst of SKR on day 059, with its accompanying extension to lower frequencies is not as clear. As noted above, both of these bursts are observed from subsolar longitudes of ~100°, around which SKR power is maximized on average, however the peak power and presence of the low-frequency component are clearly different from the surrounding days. Consequently, one interpretation is that the first SKR burst is also caused by an energetic reconnection event, but there is no detectable magnetic signature. As described by *Jackman et al.*

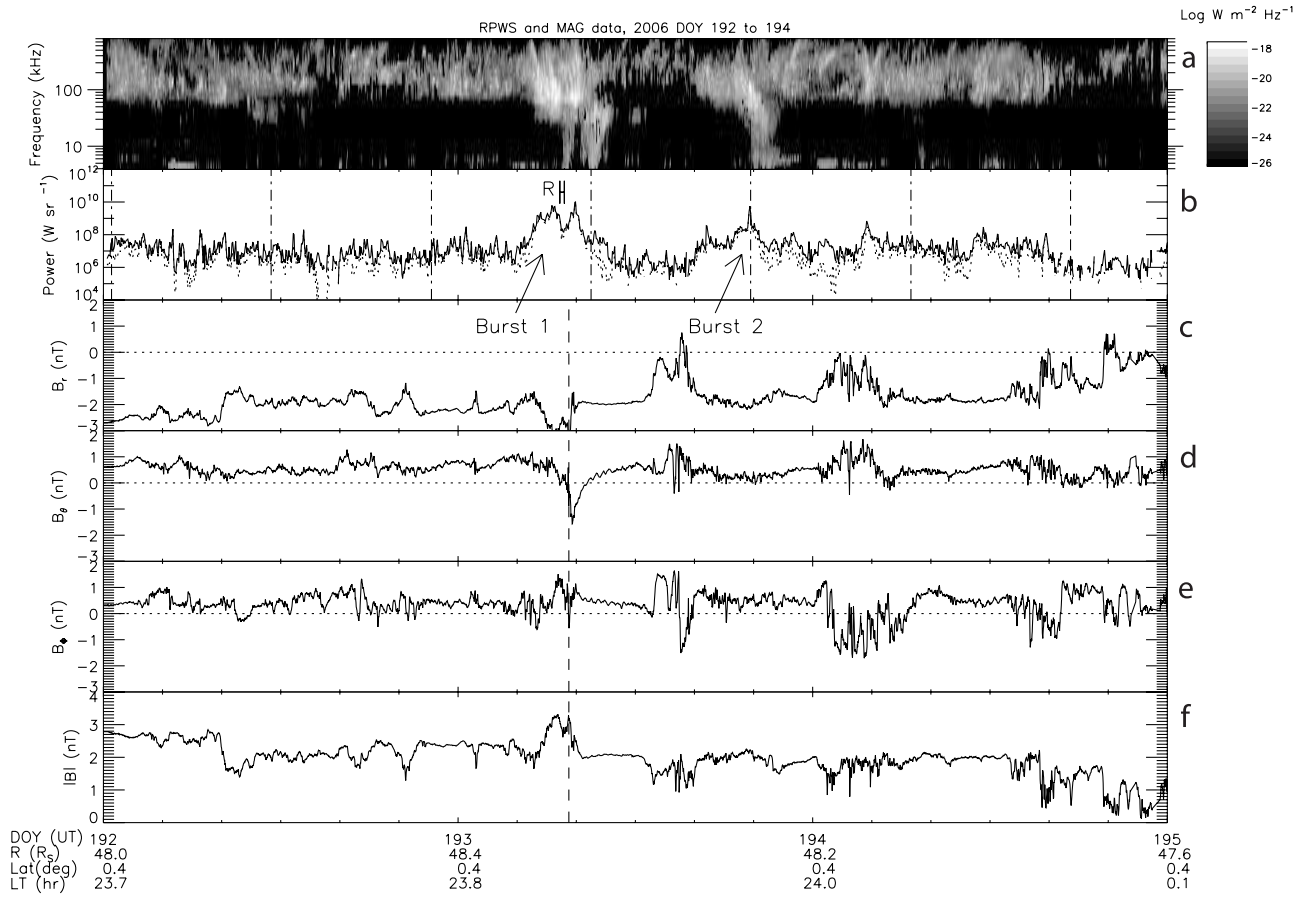

Figure 4. RPWS and MAG data from day 192–195, 2006, in the same format as Figure 2.

[2007], the search for plasmoids is hampered somewhat by the trajectory of Cassini. Owing to the hinging of the magnetotail current sheet, when the spacecraft is orbiting in the deep magnetotail at low latitudes, it may be below the nominal current sheet location, where plasmoids are most likely to be observed. The waiting time between these two LFEs appears short (~1 day) compared to the expected waiting time of 5–7 days between substorm-like events based on empirical estimates of flux addition and closure at Saturn [e.g., *Jackman et al.*, 2004]. However, we note that at Earth the most common substorm waiting time is 2–3 h even though the average waiting time is approximately 6 h, and about 4% of waiting times are less than 1 h [*Borovsky et al.*, 1993]. Alternatively, LFEs are not uniquely associated with substorms.

3.3. Example C: Day 193, 2006

[32] Figure 4 shows a third example of RPWS and MAG data from day 192–194 of 2006. The magnetic feature of interest here (marked by vertical dashed lines in Figures 4c–4f) is the northward turning of the field on day 193 (12 July) at 0730 UT, when the spacecraft was at ~48.37 R_S downtail, a LT of 23.87 h and a latitude of 0.44°. This event was discussed in detail by *Jackman et al.* [2007] who interpreted it as a signature akin to a TCR, similar to the signature shown in Figure 2.

[33] Turning to the SKR data in Figure 4a, we note that, similar to example B above, there is relatively constant emission in the ~100–400 kHz band. However, there is a very strong burst of intense emission (peaking at 1.0×10^{10} W sr^{-1}), coupled with an extension to lower frequency on day 193 starting at ~0600 UT and lasting for several hours. This peak is three orders of magnitude larger than the average power for the preceding day and occurs before the expected phasing illustrated by the vertical dashed lines in Figure 4b. Following this burst the SKR emissions fade to levels as low as $\sim 1 \times 10^6$ W sr^{-1} until a second burst just before ~2000 UT on day 193 with extension to lower frequencies, and peaking at 5.5×10^9 Wsr^{-1}. Once more, the emissions fade in the day following this event. Could these be more examples of radio emissions following compression-induced magnetic reconnection? We cannot conclusively say without the benefit of an upstream solar wind monitor, but the SKR emissions are certainly highly suggestive of a strong magnetospheric process whereby quiet radio emissions are suddenly interrupted by a very large burst of SKR. In Figure 4b, we have again plotted an error bar surrounding the interval which we suggest matches the timing of the reconnection event that produced the plasmoid. For a reconnection site at 30 R_S and a plasmoid traveling at 800 km/s to meet the spacecraft, we solve for an event time of 0706.24 UT on day 193. This time closely coincides with the center of the first radio emission burst.

3.4. Overall Correlation of SKR and Reconnection Events

[34] These three examples combine to suggest a relationship between substorm-like events and strong bursts of SKR

Table 1. Timings of Nine Reconnection Events "R" Identified With Cassini Data and Description of Their Corresponding SKR Signatures

MAG Signatures[a]	Is There SKR Enhancement Coincident With the "R" Timing Within ±1 h?	Is There an LFE Coincident With the SKR Burst Nearest the "R" Timing?	SKR Phase at "R" Timing (deg)	Are SKR Bursts in Phase With Planetary Modulation Generally?
2004 day 184 0200	yes	yes	327.96	yes, but event burst disrupts previous phasing
2006 day 060 0730	yes	yes	196.39	yes; broad bursts cover 100° longitude
2006 day 063 2258	yes	yes	222.21	yes, but event burst disrupts previous phasing
2006 day 083 1835	yes	some lower-frequency emission	234.19	minimal emission, but burst disrupts previous phasing
2006 day 085 0010	no	some lower-frequency emission	135.83	minimal emission; nearest burst occurs early
2006 day 169 0030	yes	yes	317.52	yes; event in line with previous phasing
2006 day 193 0730	yes	yes	296.69	yes; event burst early
2006 day 216 1650	yes	some lower-frequency emission	264.13	yes; event burst slightly early
2006 day 249 1530	yes	some lower-frequency emission	315.30	yes; event burst not particularly intense

[a]The three case studies discussed in this paper are shown in bold.

with extensions of the spectrum to lower frequencies. The low-frequency extensions are likely caused by accelerated electrons precipitating into the auroral zone, leading to an extension of the acceleration region and expansion of radio sources to higher altitudes. Table 1 summarizes the relationship between the nine substorm-like reconnection events that have been identified thus far from the magnetometer data and their corresponding radio emissions. The first example is from the outbound pass of SOI [*Bunce et al.*, 2005], and the other eight from the equatorial tail orbits of 2006. The three case studies shown above are indicated by asterisks. In general, there is a good correlation between the timing of a reconnection event and the observation of enhanced SKR. Further, most examples display some evidence of low-frequency extension of the spectrum, although the degree to which this is apparent varies.

[35] We also consider how these enhanced bursts fit with the planetary-modulated phasing of the SKR peaks. Do all the magnetic field signatures occur in phase with regular modulations, indicating that they may be driven by planetary-period oscillations, or if out of phase, does this suggest compression-induced tail reconnection? The fourth column of Table 1 shows the SKR phase, as defined by *Kurth et al.* [2008], at the inferred time of each of the reconnection events "R," where 0 and 360° correspond to expected SKR maximum, and 180° to SKR minimum. Eight of the nine events are clustered in the phase range of 195–360°, which is the sector of the SKR cycle where the power is expected to be rising with time on average. Thus the reconnection bursts appear to be associated with intervals where the process leading to SKR maxima is growing with time. Consequently, we suggest a substorm model in which magnetic flux accumulates in the tail for some ~5–7 days [*Jackman et al.*, 2004] to the point of some instability, but that instability is then favored at a particular phase of the planetary rotation.

[36] Despite many years of study into the terrestrial substorm-AKR correlation, and a wealth of spacecraft data, not every substorm is found to be linked to enhanced AKR emission. *Morioka et al.* [2007] derived statistics on the percentage of terrestrial substorms that provoked a change in the frequency of radio emission (where a substorm was known to have occurred). They found that 69% of examples revealed a dual- or wide-source AKR population, indicating that the appearance of a new AKR source region on a higher-altitude auroral field line is a common (but not ubiquitous) feature at substorm onset and that even the AKR is not a perfect indicator of substorm activity. The visibility effects associated with SKR analysis were introduced in section 2.1, and below we study the extensions of the spectrum to lower-frequency in a statistical manner, to aid us in deciphering the nature of the correlation with reconnection on both a general and a case-by-case basis.

4. Survey of Radio Emissions and Low-Frequency Extensions

[37] L08 presented a detailed statistical study of the general character of the bulk SKR emissions over 2.75 years since SOI. However, here we focus our attention on the extensions to low frequency in the SKR spectrum and study their typical characteristics. We first derive two strict criteria to define a "low-frequency extension" or LFE. We are interested in strong, continuous extensions of the emission to lower frequencies, as described above, and akin to the type of behavior observed for the AKR by *Morioka et al.* [2007, 2008], as distinct from the narrowband n-SMR and n-SKR emissions mentioned in section 2.2 which are produced by mechanisms other than the CMI. Consequently, we apply two criteria to define an LFE as follows: First, flux densities above a threshold of 1×10^{-25} W m^{-2} Hz^{-1} (scaled to 1 AU) must be present in the lower-frequency channels from 6.95 to 37.75 kHz). This represents emission 3 orders of magnitude above the mean and so corresponds to intense bursts. Second, the extension of the spectrum down to these lower frequencies must be continuous, i.e., no gaps in the spectrum between the lower-frequency emissions and the main SKR band (frequencies of 10.12–205.027 kHz). This ensures that periods we identify as LFEs are genuine extensions of the main auroral SKR spectrum, ruling out anomalous "blips" and the narrowband emissions n-SMR and n-SKR mentioned above.

[38] For this work, we have studied several cases of in situ reconnection events and their associated SKR signatures. By the nature of the reconnection process, we expect plasmoids to be released and travel close to the center of the current sheet. Thus our search for magnetic signatures of reconnection is largely confined to the equatorial plane. By looking statistically at the spread of LFEs during a period when we know there are several energetic reconnection

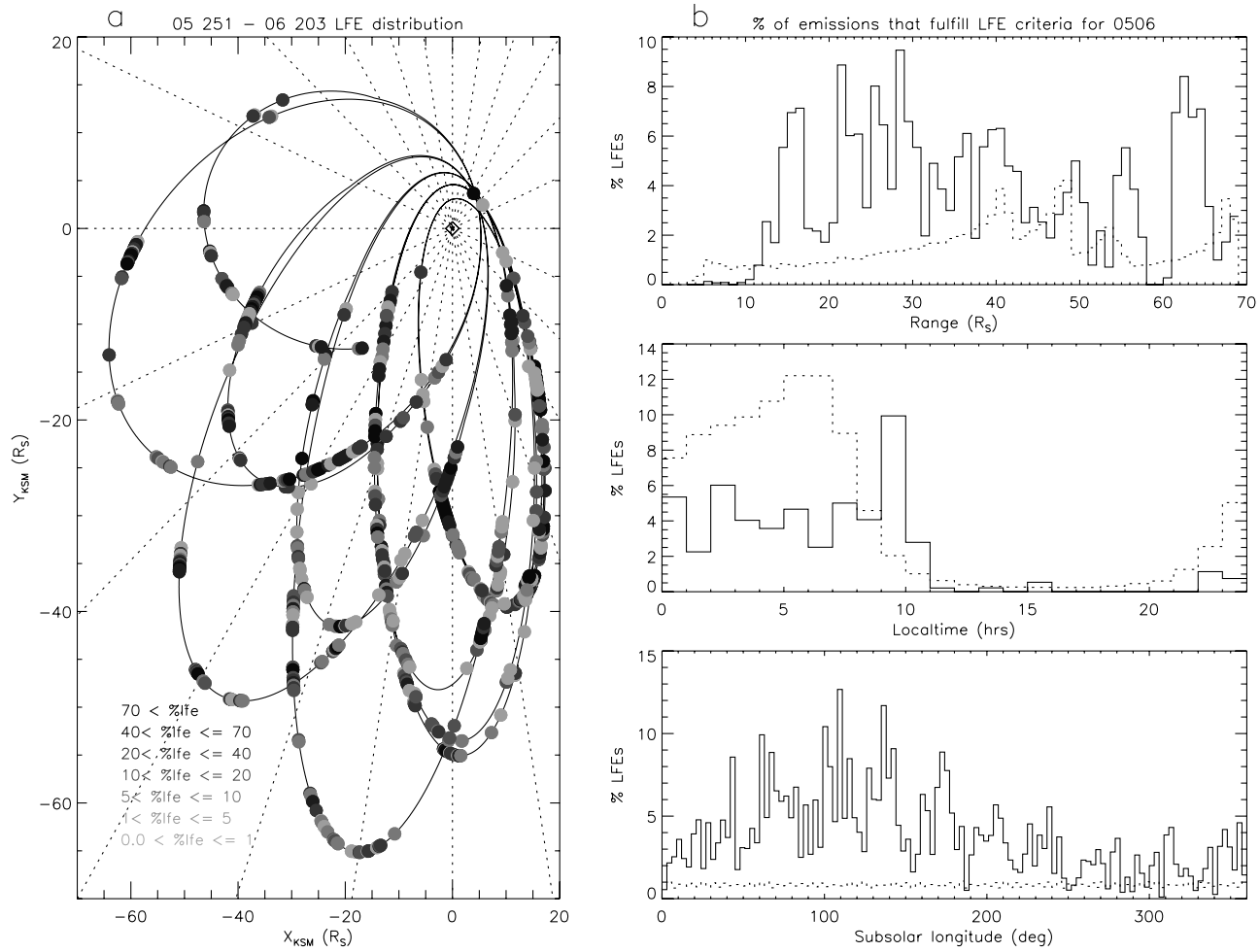

Figure 5. Distribution and statistics on low-frequency extensions (LFEs) of the SKR spectrum over the period 2005 day 251 to 2006 day 203. (a) The equatorial plane, where dotted lines mark 1 h steps in local time. Colored dots indicate the percentage of LFEs observed during each 2-h period sampled along the trajectory. Thin black trajectory traces without dots indicate periods where no LFEs were observed. (b) Histograms of the percentage of emissions that fulfill the LFE criteria as a function of radial range, local time, and subsolar longitude. The histograms of the trajectory spread in radial range, local time, and subsolar longitude are overplotted by dashed lines.

events occurring, can we separate cause and effect? Do Kronian substorms trigger bursts of SKR which extend to low frequency, or do precipitating electrons associated with reconnection merely alter the beaming of the radio emission such that it is more easily visible from certain spacecraft positions?

[39] Figures 5a and 5b show data from the portion of the Cassini orbit from 2005 day 251 to 2006 day 203, during which time the spacecraft latitude never exceeded ±0.4°. It was during these equatorial orbits that eight of the nine observed magnetic signatures of reconnection and associated plasmoids occurred. Thus, by analyzing the spread of LFE observations during this period as a subset of the nominal mission (2004–2008), we eliminate the effects of increased latitude on our statistics, and we are able to gain a better insight into how LFE visibility is affected by radial distance and local time effects in the equatorial plane.

[40] Figure 5a shows the Cassini trajectory for the interval above in the equatorial plane in KSM (cylindrical) coordinates with dotted lines for every 1 h of LT. The RPWS data over this period are at 180 s resolution. For every 2 h interval (40 points), the number of measurements fulfilling the LFE criteria as outlined above is recorded, and plotted as a dot reflecting the percentage of the number of SKR measurements in that period (always 40 assuming no data gaps). These dots are coded according to the legend on the left of the plots, such that periods with a small percentage of LFEs observed are in pale gray, with shades getting progressively darker toward black as the visibility/occurrence of the LFEs increases. Dots are omitted for periods where no LFEs were observed, so just the thin black trajectory trace is plotted during these intervals. Figure 5b shows histograms of the percentage of emissions that fulfill the low-frequency criteria as a function of radial range, LT, and subsolar longitude [*Kurth et al.*, 2008]. Overplotted by dashed lines are the histograms of trajectory information, i.e., the percentage of time spent in each R_S or radial range, each hour of LT, and each 3° wide sector of longitude.

[41] Before attempting to draw any general conclusions on the statistics, we must first consider the nature of the orbit during 2005–2006 and how this may bias our results. As mentioned above, this interval encompasses the equatorial plane only so latitude effects are not an issue. During this period, the spacecraft covered a wide range of radial distances on the nightside out to a maximum of >68 R_S on one orbit. The dayside excursions were limited to within 20 R_S of the planet. However, it is the local time effects that are most striking with a clear dawn-dusk asymmetry. The vast proportion of time was spent in the 0–10 h LT range, with only a small number of orbits exploring the dusk flank and an even smaller number in the post-noon sector at small radial distances. This scant sampling of the dusk magnetosphere at large radial distances will have an impact on the distribution of LFEs described by our statistics.

[42] L08 studied the full SKR emissions for $-1° \leq \lambda_{SC} \leq +1°$. They found that intense events with a broad spectrum are preferentially observed when the spacecraft is located between 0200 and 1100 h, and that SKR is preferentially observed from the morning side, with maximum intensity and bandwidth between 0200 and 0800 h LT. The statistics for radial distance in Figure 5b (top) show a wide spread in LFE visibility. Cassini spent on average less than 20% of its time in each of the 1 R_S-wide bins in the radial range of ~20–30 R_S, equating to less than 10% of the total period spent sampling this 10 R_S wide region. However, the number of LFEs observed from this area is significantly larger than the orbital biasing would suggest. There are several large peaks in LFE occurrence at 21–22, 25–26 and 28–29 R_S in particular, each peaking at 8% or above. The deep tail passes, particularly in the 61–65 R_S range, also have a large incidence of LFEs.

[43] The LT spread also has some striking features, including the spike in the 0900–1000 h LT range, with LFEs being observed from here almost twice as often as in any other local time sector. There is also a curious drop in the occurrence frequency of LFEs in the 0100–0200 h LT range. As mentioned above, and as is clear from Figure 5b (middle), Cassini's trajectory thus far has been biased such that it had only limited exploration of the dusk magnetosphere and a wide spread over the dawn sector. The statistics are not inconsistent with the results of L08 for the bulk SKR emission but further exploration of the dusk-side will help to better constrain visibility at all local times throughout the magnetosphere.

[44] Figure 5b (bottom) shows the spread in subsolar longitude of the LFE observations (solid line) and the trajectory itself (dashed line). Clearly the spacecraft samples all longitudes equally, so thus any biasing in the LFE histogram is a pure visibility effect. We note the on average higher occurrence frequency between ~45 and 180°, with the largest peak centered around 110° in a 3°-wide bin. This is consistent with the phasing of SKR in general, in which SKR power maximizes near 100° longitude.

[45] Overall, the spread of the LFEs appears to be similar to the spread of the bulk SKR emission, without any significant changes in visibility that may be linked in a straightforward manner to beaming effects. Thus we may interpret the LFEs in the way introduced in section 1.3, as representing expansions of the radio sources to higher altitudes along field lines.

5. Discussion and Conclusions

[46] In this paper, we have examined three case studies of in situ reconnection events in the Kronian magnetotail and their corresponding SKR signatures. For the examples shown, there is a good correlation between magnetic signatures of plasmoid passage and intense bursts of radio emission with extension to lower frequencies. The lower-frequency emission is a direct consequence of the extension of the source regions to higher altitudes, estimated up to 4 R_S, following strong energetic particle precipitation which can be driven by substorm-like events.

[47] Using magnetometer data, we have observed nine magnetic signatures of reconnection events in Saturn's magnetotail thus far. Comparing the timings of the reconnection events with the phasing of the SKR, we note that eight of the nine examples occur during the expected rising phase of the SKR cycle, which indicates the link between these events and planetary-period modulations. We suggest that Kronian substorms are a much more prevalent phenomenon than this small number of observations suggests, but our statistics are hampered by viewing geometries, namely the small amount of time that Cassini spent in the deep magnetotail near the nominal current sheet location. The three case studies we have shown represent examples with a good correlation; however, this is not the case for all events.

[48] When comparing solar wind compressions with SKR signatures while Cassini was upstream of Saturn, *Badman et al.* [2008] found that intensifications of SKR coincident with magnetospheric compressions were almost ubiquitous but that features such as "extra" peaks in the SKR spectrum and broadening of the emission were highly variable. We find that in eight of nine cases there is a good match between plasmoid timings and intensification of the SKR, however the degree of low-frequency extension is variable. We note here that while AKR intensifications have been used for many years as a proxy for terrestrial substorm activity [e.g., *Gurnett*, 1974; *Voots et al.*, 1977], they are still not a perfect indicator, in part due to diurnal modulation (L. Lamy et al., manuscript in preparation, 2009). Moreover, the LFEs we are searching for in the Kronian data set are a common but not ubiquitous feature of the terrestrial data set. *Morioka et al.* [2007] noted that the statistically derived probability of a dual- or wide-source AKR spectrum at substorm onset is ~70%. *Anderson et al.* [1997, 1998] noted that where low-frequency extensions of the AKR spectrum are seen, they are almost always accompanied by substorm onset. Certainly many examples of LFEs are observed by Cassini from a wide set of vantage points, but the spacecraft is only in the right position to observe the corresponding magnetic signature (if any) a fraction of the time. We suggest that the timescales for loading the tail with sufficient flux to trigger a substorm-like event are of the order of ~5–7 days but that the subsequent release of this energy occurs at a preferential phase of the planetary rotation.

[49] Section 4 discussed the spread of LFEs in range, latitude, and local time. Latitude effects have been shown to

be a major factor when studying the visibility of both narrowband emissions and the bulk SKR spectrum. However, we do not explore the effects of latitude on LFE visibility here. Rather with reference to Figure 5 we discuss an interval from 2005 day 251 to 2006 day 203 where Cassini sampled the equatorial plane at latitudes $\leq|0.4°|$, and during which time the magnetometer instrument detected several plasmoids traveling down the magnetotail. As outlined above, dawn-dusk asymmetries in the orbital coverage mean that the dusk magnetosphere remains largely unsampled, and thus it is not possible to make general conclusions about the occurrence or otherwise of LFEs in this region. In the absence of direct measurements, we can however make some hypotheses based on theory as to what kind of signatures may be observed in the dusk magnetosphere. At Saturn, *Cowley et al.* [2004] have modeled the Vasyliunas- and Dungey-cycle flows. In their theoretical picture, the combination of these processes makes magnetic reconnection more likely in the midnight to predawn sector of the magnetotail. Further theoretical work presented by *Cowley et al.* [2005] suggests that due to the spiral structure of the lobe field, reconnection events occurring in the center of the tail will map magnetically to later local times in the ionosphere. Thus, if magnetotail reconnection occurs more often in the midnight to predawn sector as opposed to the duskside, and if the associated field lines map to later local times in the ionosphere, we may expect this effect to be manifested in the auroral and radio response.

[50] In this paper we have demonstrated the strong correlation between substorm-like reconnection events and extensions of the SKR spectrum to lower frequencies. Further Cassini orbits in the deep magnetotail during the Cassini solstice mission beginning in 2010 should provide us with more magnetic signatures to analyze, while future orbits on the dusk flank will help to further constrain visibility issues relating to the main SKR spectrum and LFEs. Future work will also investigate both the durations and recurrence rates of LFEs with a view to placing them in the physical context of the longer intrinsic timescales of the Kronian flux addition and closure cycle.

[51] **Acknowledgments.** Work at Imperial was supported by STFC. The research at the University of Iowa was funded by NASA through contract 1279973 with the Jet Propulsion Laboratory.

[52] Amitava Bhattacharjee thanks the reviewers for their assistance in evaluating this paper.

References

Akasofu, S.-I. (1964), The development of the auroral substorm, *Planet. Space Sci.*, *12*, 273–282.

Anderson, R. R., et al. (1997), Observation of low frequency terrestrial type III bursts by Geotail and WIND and their association with isolated geomagnetic disturbances detected ground and space-borne instruments, in *Planetary Radio Emissions IV, Proc. Graz Conf.*, edited by H. O. Rucker, S. J. Buer, and A. Lecacheux, pp. 241–250, Aust. Acad. of Sci. Press, Vienna.

Anderson, R. R., et al. (1998), Geotail, Polar, CANOPUS ISTP associated geosynchronous satellite observations of plasma wave emissions and related magnetospheric phenomena during substorms, in *SUBSTORM-4*, edited by S. Kokubun and Y. Kamide, pp. 567–572, Terra Sci., Tokyo.

Angelopoulos, V., et al. (2008), Tail reconnection triggering substorm onset, *Science*, *321*(5891), 931–935, doi:10.1126/science.1160495.

Badman, S. V., S. W. H. Cowley, J.-C. Gérard, and D. Grodent (2006), A statistical analysis of the location and width of Saturn's southern aurora, *Ann. Geophys.*, *24*, 3533–3545.

Badman, S. V., S. W. H. Cowley, L. Lamy, B. Cecconi, and P. Zarka (2008), Relationship between solar wind corotating interaction regions and the phasing and intensity of Saturn kilometric radiation bursts, *Ann. Geophys.*, *26*, 3641–3651.

Benediktov, E. A., G. G. Getmansev, N. A. Mityakov, V. O. Rapoport, and A. F. Tarasov (1968), Relation between geomagnetic activity and the sporadic radio emission recorded by the electron satellites, *Cosmic Res.*, *6*, 791–794, Engl. Transl.

Borovsky, J. E., R. J. Nemzek, and R. D. Belian (1993), The occurrence rate of magnetospheric-substorm onsets: Random and periodic substorms, *J. Geophys. Res.*, *98*(A3), 3807–3813, doi:10.1029/92JA02556.

Brandt, P. C., et al. (2002), Plasma sheet dynamics during substorm from global ENA measurements onboard IMAGE, in *Sixth International Conference on Substorms*, edited by R. M. Winglee, pp. 278–282, Univ. of Wash., Seattle.

Bunce, E. J., S. W. H. Cowley, D. M. Wright, A. J. Coates, M. K. Dougherty, N. Krupp, W. S. Kurth, and A. M. Rymer (2005), In-situ observations of a solar wind compression-induced hot plasma injection in Saturn's tail, *Geophys. Res. Lett.*, *32*, L20S04, doi:10.1029/2005GL022888.

Cecconi, B., and P. Zarka (2005), Direction finding and antenna calibration through analytical inversion of radio measurements performed using a system of 2 or 3 electric dipole antennas, *Radio Sci.*, *40*, RS3003, doi:10.1029/2004RS003070.

Cecconi, B., L. Lamy, P. Zarka, R. Prangé, W. S. Kurth, and P. Louarn (2009), Goniopolarimetric study of the revolution 29 perikrone using the Cassini Radio and Plasma Wave Science instrument high-frequency radio receiver, *J. Geophys. Res.*, *114*, A03215, doi:10.1029/2008JA013830.

Clarke, J. T., et al. (2005), Morphological differences between Saturn's ultraviolet aurorae and those of Earth and Jupiter, *Nature*, *433*, 717–719, doi:10.1038/nature03331.

Cowley, S. W. H., E. J. Bunce, and J. M. O'Rourke (2004), A simple quantitative model of plasma flows and currents in Saturn's polar ionosphere, *J. Geophys. Res.*, *109*, A05212, doi:10.1029/2003JA010375.

Cowley, S. W. H., S. V. Badman, E. J. Bunce, J. T. Clarke, J.-C. Gérard, D. Grodent, C. M. Jackman, S. E. Milan, and T. K. Yeoman (2005), Reconnection in a rotation-dominated magnetosphere and its relation to Saturn's auroral dynamics, *J. Geophys. Res.*, *110*, A02201, doi:10.1029/2004JA010796.

Desch, M. D., and H. O. Rucker (1983), The relationship between Saturn kilometric radiation and the solar wind, *J. Geophys. Res.*, *88*, 8999–9006, doi:10.1029/JA088iA11p08999.

Dougherty, M. K., et al. (2004), The Cassini magnetic field investigation, *Space Sci. Rev.*, *114*, 331–383, doi:10.1007/s11214-004-1432-2.

Farrell, W. M., M. D. Desch, M. L. Kaiser, A. Lecacheux, W. S. Kurth, D. A. Gurnett, B. Cecconi, and P. Zarka (2005), A nightside source of Saturn's kilometric radiation: Evidence for an inner magnetosphere energy driver, *Geophys. Res. Lett.*, *32*, L18107, doi:10.1029/2005GL023449.

Fok, M.-C., T. E. Moore, P. C. Brandt, D. C. Delcourt, S. P. Slinker, and J. A. Fedder (2006), Impulsive enhancements of oxygen ions during substorms, *J. Geophys. Res.*, *111*, A10222, doi:10.1029/2006JA011839.

Green, J. L., D. A. Gurnett, and S. D. Shawhan (1977), The angular distribution of auroral kilometric radiation, *J. Geophys. Res.*, *82*, 1825–1838, doi:10.1029/JA082i013p01825.

Gurnett, D. A. (1974), The Earth as a radio source: Terrestrial kilometric radiation, *J. Geophys. Res.*, *79*, 4227–4238.

Gurnett, D. A., W. S. Kurth, and F. L. Scarf (1981), Narrowband electromagnetic radiation from Saturn's magnetosphere, *Nature*, *292*, 733–737, doi:10.1038/292733a0.

Gurnett, D. A., et al. (2004), The Cassini radio and plasma wave investigation, *Space Sci. Rev.*, *114*, 395–463, doi:10.1007/s11214-004-1434-0.

Hill, T. W., et al. (2008), Plasmoids in Saturn's magnetotail, *J. Geophys. Res.*, *113*, A01214, doi:10.1029/2007JA012626.

Jackman, C. M., N. Achilleos, E. J. Bunce, S. W. H. Cowley, M. K. Dougherty, G. H. Jones, S. E. Milan, and E. J. Smith (2004), Interplanetary magnetic field at ~9 AU during the declining phase of the solar cycle and its implications for Saturn's magnetospheric dynamics, *J. Geophys. Res.*, *109*, A11203, doi:10.1029/2004JA010614.

Jackman, C. M., N. Achilleos, E. J. Bunce, B. Cecconi, J. T. Clarke, S. W. H. Cowley, W. S. Kurth, and P. Zarka (2005), Interplanetary conditions and magnetospheric dynamics during the Cassini orbit insertion fly through of Saturn's magnetosphere, *J. Geophys. Res.*, *110*, A10212, doi:10.1029/2005JA011054.

Jackman, C. M., C. T. Russell, D. J. Southwood, C. S. Arridge, N. Achilleos, and M. K. Dougherty (2007), Strong rapid dipolarizations in Saturn's magnetotail: In situ evidence of reconnection, *Geophys. Res. Lett.*, *34*, L11203, doi:10.1029/2007GL029764.

Jackman, C. M., et al. (2008), A multi-instrument view of tail reconnection at Saturn, *J. Geophys. Res.*, *113*, A11213, doi:10.1029/2008JA013592.

Jackman, C. M., C. S. Arridge, H. J. McAndrews, M. G. Henderson, and R. J. Wilson (2009), Northward field excursions in Saturn's magnetotail

and their relationship to magnetospheric periodicities, *Geophys. Res. Lett.*, doi:10.1029/2009GL039149, in press.

Kaiser, M. L., and J. K. Alexander (1977), Terrestrial kilometric radiation: 3. Average spectral properties, *J. Geophys. Res.*, *82*, 3273–3280.

Kaiser, M. L., M. D. Desch, J. W. Warwick, and J. B. Pearse (1980), Voyager detection of non-thermal radio emission from Saturn, *Science*, *209*, 1238–1240, doi:10.1126/science.209.4462.1238.

Kaiser, M. L., M. D. Desch, W. S. Kurth, A. Lecacheux, F. Genova, B. M. Pedersen, and D. R. Evans (1984), Saturn as a radio source, in *Saturn*, edited by T. Gehrels and M. S. Matthews, 378 pp., Univ. of Ariz. Press, Tucson.

Khurana, K. K., D. G. Mitchell, C. S. Arridge, M. K. Dougherty, C. T. Russell, C. Paranicas, N. Krupp, and A. J. Coates (2009), Sources of rotational signals in Saturn's magnetosphere, *J. Geophys. Res.*, *114*, A02211, doi:10.1029/2008JA013312.

Knight, S. (1973), Parallel electric fields, *Planet. Space Sci.*, *21*, 741–750, doi:10.1016/0032-0633(73)90093-7.

Kronberg, E. A., J. Woch, N. Krupp, A. Lagg, K. K. Khurana, and K.-H. Glassmeier (2005), Mass release at Jupiter: Substorm-like processes in the Jovian magnetotail, *J. Geophys. Res.*, *110*, A03211, doi:10.1029/2004JA010777.

Kronberg, E. A., K.-H. Glassmeier, J. Woch, N. Krupp, A. Lagg, and M. K. Dougherty (2007), A possible intrinsic mechanism for the quasi-periodic dynamics of the Jovian magnetosphere, *J. Geophys. Res.*, *112*, A05203, doi:10.1029/2006JA011994.

Krupp, N., J. Woch, A. Lagg, B. Wilken, S. Livi, and D. J. Williams (1998), Energetic particle bursts in the predawn Jovian magnetotail, *Geophys. Res. Lett.*, *25*, 1249–1252, doi:10.1029/98GL00863.

Kurth, W. S., M. M. Baumback, and D. A. Gurnett (1975), Direction-finding measurements of auroral kilometric radiation, *J. Geophys. Res.*, *80*, 2764–2770, doi:10.1029/JA080i019p02764.

Kurth, W. S., et al. (2005), An Earth-like correspondence between Saturn's auroral features and radio emission, *Nature*, *433*, 722–725, doi:10.1038/nature03334.

Kurth, W. S., T. F. Averkamp, D. A. Gurnett, J. B. Groene, and A. Lecacheux (2008), An update to a Saturnian longitude system based on kilometric radio emissions, *J. Geophys. Res.*, *113*, A05222, doi:10.1029/2007JA012861.

Lamy, L. (2008), Study of radio auroral emissions of Saturn, modelling and UV auroras, Ph.D. thesis, Univ. Pierre et Marie Curie, Meudon, France.

Lamy, L., P. Zarka, B. Cecconi, R. Prangé, W. S. Kurth, and D. A. Gurnett (2008), Saturn kilometric radiation: Average and statistical properties, *J. Geophys. Res.*, *113*, A07201, doi:10.1029/2007JA012900.

Louarn, P., A. Roux, S. Perraut, W. S. Kurth, and D. A. Gurnett (1998), A study of the large-scale dynamics of the Jovian magnetosphere using the Galileo plasma wave experiment, *Geophys. Res. Lett.*, *25*, 2905–2908, doi:10.1029/98GL01774.

Louarn, P., A. Roux, S. Perraut, W. S. Kurth, and D. A. Gurnett (2000), A study of the Jovian "energetic magnetospheric events" observed by Galileo: Role in the radial plasma transport, *J. Geophys. Res.*, *105*, 13,073–13,088, doi:10.1029/1999JA900478.

Louarn, P., et al. (2007), Observation of similar radio signatures at Saturn and Jupiter, implications for the magnetospheric dynamics, *Geophys. Res. Lett.*, *34*, L20113, doi:10.1029/2007GL030368.

Mitchell, D. G., P. C. Brandt, E. C. Roelof, D. C. Hamilton, K. C. Retterer, and S. Mende (2003), Global imaging of O+ from IMAGE/HENA, *Space Sci. Rev.*, *109*, 63–75, doi:10.1023/B:SPAC.0000007513.55076.00.

Mitchell, D. G., et al. (2005), Energetic ion acceleration in Saturn's magnetotail: Substorms at Saturn?, *Geophys. Res. Lett.*, *32*, L20S01, doi:10.1029/2005GL022647.

Morioka, A., Y. Miyoshi, F. Tsuchiya, H. Misawa, T. Sakanoi, K. Yumoto, R. R. Anderson, J. D. Menietti, and E. F. Donovan (2007), Dual structure of auroral acceleration regions at substorm onsets as derived from auroral kilometric radiation spectra, *J. Geophys. Res.*, *112*, A06245, doi:10.1029/2006JA012186.

Morioka, A., et al. (2008), AKR breakup and auroral particle acceleration, *J. Geophys. Res.*, *113*, A09213, doi:10.1029/2008JA013322.

Mutel, R. L., I. W. Christopher, and J. S. Pickett (2008), Cluster multi-spacecraft determination of AKR angular beaming, *Geophys. Res. Lett.*, *35*, L07104, doi:10.1029/2008GL033377.

Nakamura, R., et al. (2002), Fast flow during current sheet thinning, *Geophys. Res. Lett.*, *29*(23), 2140, doi:10.1029/2002GL016200.

Russell, C. T., and R. L. McPherron (1973), The magnetotail and substorms, *Space Sci. Rev.*, *15*, 205–266, doi:10.1007/BF00169321.

Slavin, J. A., E. J. Smith, B. T. Tsurutani, D. G. Sibeck, H. J. Singer, D. N. Baker, J. T. Gosling, E. W. Hones, and F. L. Scarf (1984), Substorm associated travelling compression regions in the distant tail: ISEE-3 GEOTAIL observations, *Geophys. Res. Lett.*, *11*, 657–660, doi:10.1029/GL011i007p00657.

Taubenschuss, U., H. O. Rucker, W. S. Kurth, B. Cecconi, P. Zarka, M. K. Dougherty, and J. T. Steinberg (2006), Linear prediction studies for the solar wind and Saturn kilometric radiation, *Ann. Geophys.*, *24*, 3139–3150.

Voots, G. R., D. A. Gurnett, and S.-I. Akasofu (1977), Auroral kilometric radiation as an indicator of auroral magnetic disturbances, *J. Geophys. Res.*, *82*, 2259–2266, doi:10.1029/JA082i016p02259.

Woch, J., N. Krupp, A. Lagg, B. Wilken, S. Livi, and D. J. Williams (1998), Quasi-periodic modulations of the Jovian magnetotail, *Geophys. Res. Lett.*, *25*, 1253–1256, doi:10.1029/98GL00861.

Wu, C. S., and L. C. Lee (1979), A theory of the terrestrial kilometric radiation, *Astrophys. J.*, *230*, 621–626, doi:10.1086/157120.

Ye, S.-Y., D. A. Gurnett, G. Fischer, B. Cecconi, J. D. Menietti, W. S. Kurth, Z. Wang, G. B. Hospodarsky, P. Zarka, and A. Lecacheux (2009), Source locations of narrowband radio emissions detected at Saturn, *J. Geophys. Res.*, *114*, A06219, doi:10.1029/2008JA013855.

Zarka, P., B. Cecconi, and W. S. Kurth (2004), Jupiter's low-frequency radio spectrum from Cassini/Radio and Plasma Wave Science (RPWS) absolute flux density measurements, *J. Geophys. Res.*, *109*, A09S15, doi:10.1029/2003JA010260.

B. Cecconi, L. Lamy, and P. Zarka, LESIA, Observatoire de Paris, UPMC, CNRS, Université Paris Diderot, Meudon, France.

S. W. H. Cowley, Department of Physics and Astronomy, University of Leicester, Leicester LE1 7RH, UK.

M. K. Dougherty and C. M. Jackman, Blackett Laboratory, Imperial College London, London SW7 2BW, UK.

M. P. Freeman, British Antarctic Survey, High Cross, Madingley Road, Cambridge CB3 0ET, UK.

W. S. Kurth, Department of Physics and Astronomy, University of Iowa, Iowa City, IA 52242, USA.